MELCOR analysis of OSU multi-application small light water reactor (MASLWR) experiment

Dhongik S. Yoon[a,*], HangJin Jo[a], Wen Fu[b], Qiao Wu[c], and Michael L. Corradini[a]

[a] Department of Engineering Physics, University of Wisconsin, 1500 Engineering Drive, Madison, WI 53706, USA

[b] Institute of Nuclear and New Energy Technology, Tsinghua University, Beijing 100084, China

[c] School of Nuclear Science and Engineering, Oregon State University, 151 Batcheller Hall, Corvallis, OR 97331, USA

Total number of pages: 41

Total number of tables: 6

Total number of figures: 14

Submitted to:

Nuclear Technology

*Corresponding author:

Dhongik S. Yoon

Tel.: 1-414-331-9168

Email address: dsyoon@wisc.edu

Mailing address: 839 Engineering Research Building, 1500 Engineering Dr., Madison WI, 53706

ABSTRACT

A multi-application small light water reactor (MASLWR) conceptual design was developed by Oregon State University (OSU) with emphasis on passive safety systems. The passive containment safety system employs condensation and natural circulation to achieve the necessary heat removal from the containment in case of postulated accidents. Containment condensation experiments at the MASLWR test facility at OSU are modeled and analyzed with MELCOR, a system-level reactor accident analysis computer code. The analysis assesses its ability to predict condensation heat transfer in the presence of noncondensable gas for accidents where high-energy steam is released into the containment. This work demonstrates MELCOR's ability to predict the pressure-temperature response of the scaled containment. Our analysis indicates that the heat removal rates are underestimated in the experiment due to the limited locations of the thermocouples and applies corrections to these measurements by conducting integral energy analyses along with CFD simulation for confirmation. The corrected heat removal rate measurements and the MELCOR predictions on the heat removal rate from the containment show good agreement with the experimental data.

Keywords: condensation, multi-application small light water reactor, MELCOR

I. INTRODUCTION

Since the inception of nuclear power, consideration of postulated accidents to assure safe operation and minimal releases of effluents has been a central focus. The containment surrounding the nuclear steam supply system must be designed to withstand the release of any high-pressure, high-temperature steam to maintain the integrity of the structure. Condensation on the containment inner walls provides heat transfer via phase change and needs to be considered as a primary energy removal mechanism from the containment in case of accidents as it achieves the necessary energy removal without the need for emergency cooling pumps and/or offsite power [1].

In current designs, air is present in the containment and, in the case of severe accidents, hydrogen gas may also be produced by metal oxidation. This presence of noncondensable gas in the containment poses the adverse effect for condensation [2] as steam condenses on the cold wall, noncondensable gas builds up near the wall region and acts as another layer of mass transfer resistance through which steam must diffuse in order to condense. So the presence of noncondensable gas not only complicates the mechanism but also hinders the magnitude of heat transfer associated with it. Therefore, the ability to predict the temperature-pressure response in the containment under condensation with the presence of noncondensable gas is critical regarding reactor design with passive safety systems.

Current analysis of condensation in the presence of noncondensable gas has two major approaches: analytical models and phenomenological models. Analytical models offer first-principle based solutions by directly solving conservation laws simplified via series of assumptions (typically including no-slip wall, negligible shear forces at liquid-vapor interface, etc.) [3-4]. Later models are further refined with consideration of turbulence [5-9] and by introducing different approaches such as diffusion layer theory [10-12]. Today, with more computing powers available, more holistic approaches with fewer assumptions via computational fluid dynamics (CFD) may be taken.

Phenomenological models are significantly less sophisticated, while capturing the key phenomena, and therefore are computationally less expensive while providing reasonable results. The heat and mass transfer analogy (HMTA) is more widely used theoretical basis for most phenomenological models for condensation. Chilton and Colburn [13] proposed a relation between mass transfer and heat transfer, for fully turbulent flows, stating that the process in which material is transferred by diffusion are closely related to heat transfer, since the latter can be considered merely as the diffusion of hot molecules into a region of cold ones and vice versa. The analogy, if appropriately applied, showed reasonable agreement with experimental data and was expanded by many researchers to fit a range of specific conditions [14-17]. The models are improved by correction factors addressing physical phenomena significantly affecting the process of condensation that are not considered in the original formulations of HMTA [14, 18-19]. Ambrosini [20] summarized various forms of the analogy to clarify their assumptions and evaluate the related differences.

Reactor systems codes provide complete system analyses for integrated predictions of system behavior in the nuclear power plant. Because the analyses are often transient and include many different reactor components, they rely on computationally inexpensive phenomenological models based on HMTA when dealing with condensation heat transfer. It was observed through the previous assessment of the two more widely used systems codes, RELAP5-3D and MELCOR, that MELCOR analyses are more reliable when dealing with containment condensation with the presence of noncondensable gas [21] so this work uses the MELCOR code as the primary analysis tool for integral steam condensation tests.

Containment condensation experiments at multi-application small light water reactor (MASLWR) facility at Oregon State University (OSU) are modeled and analyzed with MELCOR. The MASLWR integral reactor concept, developed by Idaho National Engineering and Environmental Laboratory, OSU and NEXANT-Bechtel, takes advantage of condensation and natural circulation to achieve the necessary energy removal from containment in case of accidents for pressurized steam escaping into the containment [22]. The MASLWR facility at OSU models the conceptual MASLWR design through which a series of

experiments to test containment heat transfer processes was conducted. The experiments can be used to validate reactor systems codes for accident analysis and to give insights to the passive safety systems in newer reactor designs. In this work, we evaluate the overall performance of the MELCOR system code in predicting the behavior of the MASLWR containment condensation experiments at OSU. MELCOR version 2.1 is used for all analysis directly discussed in this paper.

II. DESCRIPTION OF EXPERIMENTS

II.A. Test Facility

The MASLWR facility at OSU models the conceptual MASLWR design including the reactor cavity and containment structure [1]. It is scaled at 1:3 length scale and 1:255 volume scale, and designed to withstand full prototype operational pressure and temperature (11.4 MPa and 590 K) [23]. The facility contains three major components: the primary circuit which includes the reactor pressure vessel (RPV) and its internal components, secondary circuit mainly composed of steam generator and feed water components, and the containment structure [1]. This paper focuses on the analysis of the temperature-pressure response of the containment structure as high energy steam is injected into it.

Fig. 1 represents the containment structure components. The containment structure includes high pressure containment (HPC) and cooling pool vessel (CPV) connected by rectangular heat transfer plate (marked as condensation interface in Fig. 1). The HPC is a 5.75-m cylindrical tower. Upper section of the HPC has larger diameter than the lower section and two sections are connected with eccentric cone section. The CPV, which represents the water in which the whole reactor system is submerged [1], is a 7.37-m cylindrical tower with free surface on top filled completely with room temperature water. The heat transfer plate is 16.8 cm wide, 3.81-cm thick and axially covers the entire length of the HPC [1]. The plate connects the HPC and the CPV axially and acts as the only heat sink from the containment. Side and top view of the containment system are shown in Fig. 2, 3, respectively, and Table 1 summarizes detailed dimensions of the containment structure. The heat transfer plate is marked as the black-shaded area in Fig. 2 and 3.

II.B. Experiment Conditions

The containment condensation tests examine the quasi steady state behavior of the containment with backward facing step steam input as shown in Fig. 4. In the beginning, the HPC, initially only containing room temperature air, is filled with steam superheated at approximately 2.1 MPa and 530 K at a constant flow rate. Later, the steam flow rate is reduced and held constant at the lowered rate to maintain the containment pressure. The transient containment pressure corresponding to the steam inlet flow rate is also shown in Fig. 4. Two tests with different initial containment conditions are analyzed with MELCOR in this paper: near vacuum and atmospheric condition. The initial and steady state conditions for considered tests are summarized in Table 2. Molar and mass fraction (represented as *X* and *Y*, respectively) of noncondensable gas during the quasi steady state are estimated using ideal gas assumption as outlined in following equations. *N* and *M* represents number of moles and molar mass, respectively.

$$N_j \propto \frac{P_j}{T_j} \tag{1}$$

$$X_g = \frac{N_o}{N_{ss}} = \frac{P_o T_{ss}}{P_{ss} T_o}; X_s = 1 - X_g \tag{2}$$

$$Y_g = \frac{M_g X_g}{M_g X_g + M_s X_s} \tag{3}$$

II.C. Uncertainty Analysis

The heat flux from the HPC to CPV was computed using the array of the thermocouples embedded in the heat transfer plate by Fourier's law of conduction.

$$q'' = \left(k \frac{\Delta T}{\delta}\right)_w \tag{4}$$

Providing the uncertainties for each measurement, the overall uncertainties for the heat flux measurements is approximately 5% using the following expression for the propagation of error, with the highest local error of 11%.

$$\frac{\sigma_q}{q''} = \sqrt{\left(\frac{\sigma_k}{k}\right)^2 + 2\left(\frac{\sigma_T}{T}\right)^2 + \left(\frac{\sigma_\delta}{\delta}\right)^2} \approx 0.05 \tag{5}$$

The reported uncertainties for the measurements are summarized in Table 3.

III. MODELING OF THE EXPERIMENT

MELCOR uses the control volume hydrodynamics (CVH) package to model thermal-hydraulic behavior via control volume approach [25]. The control volume representation of the actual cylindrical containment does not contain all its geometric characteristics and only retains flow characteristics such as cell volume as a linear function of altitude, hydraulic diameter, etc. The heat structure (HS) package models one-dimensional conduction in solid material [25].

The containment structure is represented in collection of control volumes as shown in Fig. 3. Both the HPC and the CPV are nodalized to have two control volumes at each axial height to allow for natural circulation. Maintaining the two-column division for natural circulation flow, finer nodalizations of the structure were also studied to confirm nodalization-independent results. Rectangular heat structures are used to model the heat transfer plate connecting the HPC and the CPV (black-shaded blocks in Fig. 3). And cylindrical shell heat structures (gray-shaded blocks in Fig. 3) are placed outside of the HPC control volumes wall with adiabatic exterior boundary condition to account for the heating of containment vessel. Both the HPC and CPV are covered with insulation material and electric heater is attached to the outer shell of the HPC to account for the heat loss. For the simplicity of simulation, insulation materials and electric heaters were ignored and adiabatic boundary conditions were used for outermost surfaces exposed to ambient surroundings.

To simulate free surface on top of the CPV, two hypothetical control volumes are placed on top of the CPV tank. The first control volume, CV-A1 in Fig. 3, initially filled with air at ambient condition is placed on top of the uppermost CPV control volumes allowing flow to and from them so that the CPV water level can change via water flow upward or air flow downward. Properties of CV-A1, such as temperature,

pressure and composition, can change over time in case of water level rise or drop. The second control volume, CV-A2, is defined as time-independent and acts as the ambient surroundings. Its properties remain unchanged even though the flow from or to the control volume occurs. In control volume stand point of view, this stacking of surroundings control volumes guarantee necessary water level change in case of water total volume change.

IV. CONDENSATION MODEL WITH HMTA

The HMTA has its roots on Chilton and Colburn's j-factor analogy, which relates the heat and mass transfer to turbulent momentum transfer. The explicit formulation was suggested as the following [13].

$$\frac{f}{2} = j_H = \frac{h/c_p}{\rho u} \cdot Pr^{2/3} = j_M = \frac{K}{\rho u} \cdot Sc^{2/3} \tag{4}$$

The friction factor (*f*) is proportional to the transfer factors (*j*), which represent the ratio of the transfer rate of quantity of interest (h/c_p and $K=h_m\rho$ for heat and mass transfer quantity, respectively) and the mass flux of the bulk flow (ρu) multiplied by the relevant non-dimensional number raised to some power. The Prandtl number and Schmidt number, representing the ratio of resistance to heat or mass transfer to the momentum transfer, are used for heat and mass transfer factor, respectively. As shown in the formulations. the analogy assumes that the basic mechanisms of heat and mass transfer are similar and relates the heat and mass transfer. It was indicated that the power of 2/3 in equation 4 are derived from correlations of data on heat transfer [13]. Table 4 summarizes the analogous parameters in heat and mass transfer.

To obtain the explicit expression for mass transfer, specifically for condensation in this case, it is better to re-write the equation 4 as follows. k, L, ρ, c_p, μ and D represent thermal conductivity, characteristic length scale, density, heat capacity, dynamic viscosity and mass diffusivity, respectively.

$$j_H = \frac{h/c_p}{\rho u} \cdot Pr^{2/3} = \left(\frac{hL}{k}\right)\left(\frac{\mu}{\rho u L}\right)\left(\frac{k}{c_p \mu}\right) Pr^{2/3} = \frac{Nu}{RePr^{1/3}} \tag{5}$$

$$j_M = \frac{K}{\rho u} \cdot Sc^{2/3} = \left(\frac{h_m L}{D}\right)\left(\frac{\mu}{\rho u L}\right)\left(\frac{\rho D}{\mu}\right) Sc^{2/3} = \frac{Sh}{ReSc^{1/3}} \tag{6}$$

$$j_H = j_M = \frac{Nu}{Pr^{1/3}} = \frac{Sh}{Sc^{1/3}} \tag{7}$$

This general formulation for the HMTA (equation 7) is obtained from equating equation 5 and 6 and applicable in both natural and forced convection flow regimes. Although the HMTA assumes fully turbulent flow [13], MELCOR applies HMTA even for laminar flows [25]. Reynolds number and Rayleigh numbers defines the laminar/turbulence and natural/forced convection regimes, respectively and according to the flow regime, MELCOR applies appropriate correlations. Rearranging equation 7 provides following expression for Sherwood number. MELCOR uses the exact same expression for computing Sherwood number (equation 8). Any by the definition of Sherwood number, the mass transfer coefficient can be obtained accordingly.

$$Sh = NuPr^{-1/3}Sc^{1/3} \tag{8}$$

$$h_m \equiv Sh\frac{D}{L} \tag{9}$$

Now that the mass transfer coefficient is known, the complete expression for condensation mass transfer can be obtained from the diffusion theory. At the liquid-vapor interface where condensation occurs, the average molar velocity of noncondensable gas can be expressed as below, where *c* and *J* represent molar density and molar flux, respectively. *n* denotes a normal direction.

$$cu_{gi} = cX_{gi}u_i - J_g = cX_{gi}u_i - cD\frac{\partial X_g}{\partial n} \tag{10}$$

Because the interface is impermeable to the noncondensable gas, the velocity of noncondensable gas is zero ($u_{gi} = 0$). And assuming relatively linear gradient in the diffusion layer thickness of $\delta_d = D/h_m$, the expression for mixture velocity at the interface can be estimated.

$$u_i = \frac{D}{X_g}\frac{\partial X_g}{\partial n} = D\frac{\partial}{\partial n}\left(\ln\left(X_g\right)\right) = \frac{D}{\delta_d}\left(\ln\left(X_{gb}\right) - \ln\left(X_{gi}\right)\right) = h_m\left(ln\left(X_{gb}\right) - ln\left(X_{gi}\right)\right) \tag{11}$$

The rate of condensation in terms of condensation mass flux (*G*) can be expressed as below:

$$G_c = -M_s(cX_{si}u_i - J_s) = -\mathrm{M_s}\left(cX_{si}u_i + J_g\right) = -M_s\left(cX_{si}u_i + cX_{gi}u_i\right) = -cM_s u_i \tag{12}$$

The final expression for the rate of condensation can then be obtained by combining equation 11 and 12 with replacing the molar fraction terms to partial pressures.

$$G_c = -h_m\rho_{sb}\left(ln\left(\frac{P_{gb}}{P_b}\right) - ln\left(\frac{P_{gi}}{P_b}\right)\right) = h_m\rho_{sb}\left(\frac{ln(P_b - P_{si})}{ln(P_b - P_{sb})}\right) \tag{13}$$

Heat transfer rate due to condensation can then be calculated using the enthalpy change associated with phase chance (I_{fg}).

$$q_c'' = I_{fg}G_c \tag{14}$$

Therefore, with parameters for heat transfer known, the rate of condensation, and heat transfer rate associated with it, can be obtained using equation 9, 13 and 14. This analysis assumes that the mixture is relatively dilute and the condensation gradient is linear in a relatively thin diffusion layer. MELCOR uses this exact model. This diffusion model does not directly solve the conservation laws. However, in most cases of nuclear application, the model has been proven to provide reasonable predictions [13-17, 20-21].

V. RESULTS

V.A. Primary Simulation Results

MELCOR predicted containment pressure and temperature for each test are illustrated in Fig. 5 and 6. Following the initial transient phase, quasi steady state is observed where the thermodynamic conditions stay relatively constant. Fig. 7 shows heat flux through the heat transfer plate from the startup of the experiment for Test 1 at a fixed elevation. It is observed that the heat removal rate through the heat transfer

plate also stays flat during the quasi steady state period. Time averaged heat fluxes at different axial locations during the quasi steady state are summarized in Table 5.

Using the experimentally reported steam injection rates and the initial conditions for the experiments, MELCOR simulation well predicts the temperature-pressure response of the containment. However, it provides apparent overestimations of the heat removal rate from the HPC through the heat transfer plate for all locations and tests. In other words, with a given steam injection rate, the transient temperature and pressure are predicted by the MELCOR simulation with reasonable accuracy and yet the heat removal rate is always significantly overestimated. The ratios of predicted and measured heat fluxes at difference axial locations, summarized in Table 5, indicate that MELCOR always overestimates the heat flux by a seemingly constant factor of approximately 1.63. Fig. 8 shows the ratio of predicted and measured heat flux at different axial locations for both tests.

V.B. Effect of Two-Dimensional Heat Flow

Even though the edges of the heat transfer plate exposed to the surroundings are well insulated and therefore heat loss from the edges are negligible, the energy released from the containment can be transferred through the edges touching the CPV outer vessel wall via conduction. The heat conducted to the CPV outer vessel wall would then be deposited into the water pool. The heat flux measurements, calculated using the temperature gradient from the thermocouples (marked as black dots in Fig. 9), therefore does not well represent the actual total heat transfer through the plate because the thermocouples are only placed in the centerline. Because the heat flow to the outer vessel wall cannot be measured by the setup of the thermocouples, the heat flux measurements in this setup would always be an underestimation of the actual heat transfer as do the current MELCOR results suggest.

As mentioned earlier, based on the seemingly constant ratio of MELCOR predicted and measured heat flux, it was postulated that the effect of the two-dimensional heat flow depends only on the geometry and can be expressed in terms of the heat flux (q'') measured at the centerline of the heat transfer plate.

$$q_a'' \approx R q_m'' \; ; \; R \neq f(H, q'') \tag{15}$$

Table 6 shows the result of integral energy balance from the experimental data assuming negligible heat loss to the surroundings. From the integral energy balance, theoretical rate of heat removal can be calculated and the ratio of theoretical and measured heat flux can be estimated as expressed in equation 16. The thermal properties of incoming steam are outlined in Table 2 and the properties of water condensate film were obtained from the HPC pressure and near-wall fluid temperature data from the experiment. The result of the integral energy balance is shown in Fig. 10.

$$R \approx \frac{q_a''}{q_m''} = \frac{\dot{m}_s(i_s - i_f)}{A_p} \cdot \frac{1}{q_m''} \tag{16}$$

The ratio of theoretical and measured rate of heat transfer is calculated to be 1.63 in average which matches with the ratio calculated with MELCOR predicted values. However, for each test, the ratio shows clear difference; 1.73 and 1.53 for Test 1 and 2, respectively. The only difference between Test 1 and 2 in heat removal rate stand point of view is the incoming heat flux which suggests that the ratio may be dependent on the incoming heat flux.

Although the MELCOR predictions did not show this incoming heat flux dependence, the MELCOR prediction of heat removal rate from the HPC deposited into the CPV still generally agrees with the theoretical rate of heat transfer calculated from the energy balance with up to 15 % deviation at most. The measured heat flux data are always underestimating because of the limitation posed by the location of thermocouples in the heat transfer plate.

In order to confirm the results from the integral energy balance and to investigate heat flux dependence, computational fluid dynamics (CFD) analysis on two-dimensional heat flow was conducted with ANSYS Fluent v16.2. This analysis assumes that the incoming heat flow on the containment side is unidirectional and the two-dimensionality rises from the presence of CPV outer vessel wall enhancing heat transfer resembling fin effect. The transient period in the beginning of the test prior to the drop in steam

inlet flow rate was ignored and the time-averaged heat flux value at during the quasi steady state period was used to examine the digressing heat flow due to the geometry.

Fig. 11 shows the temperature distribution in water pool, CPV outer vessel wall and the heat transfer plate as a result of the CFD simulation. The CPV vessel wall is indeed heated and there exists significant temperature gradient on near vessel wall region, confirming two-dimensional heat flow. The ratio of the actual and centerline heat flux from the CFD simulation for both tests are shown in Fig. 12. We observed that the CFD simulation reproduces the result from the integral energy balance within reasonably small deviation, confirming that the measured heat flux is indeed not a good representation of the actual heat removal rate from the containment. Time-averaged ratios from the local peak during the quasi steady state period are calculated to be 1.70 for both Test 1 and 2.

The CFD results suggest that the ratio of actual and centerline heat flux is not dependent on the magnitude of incoming heat flux whereas it was observed, through the integral energy balance, that the ratio was greater with larger incoming heat flux. The disagreement between the CFD simulation results and integral energy balance results are under 10% which suggest that the heat flux dependence of integral energy balance results may be from uncertainties in measurements and errors due to spatial averaging process. However, larger set of tests with different containment conditions is needed to further investigate the heat flux dependence of the effect of two-dimensional heat flow. Nevertheless, it is apparent that the measured heat flux is an underestimation of the actual heat transfer rate and therefore is not a good representation of the actual systems behavior.

The heat flux measurements are then corrected by applying the ratio of actual and measured heat flux computed via energy balance (EB) and CFD. The analysis results for Test 1 and 2 comparing the MELCOR results with the corrected measurements are presented in Fig. 13 and 14, respectively. MELCOR predictions generally agree well with the corrected experimental heat flux data. The average deviations from the corrected data are around 5% and, at most, 11%. Considering the additional errors from the correction methods, MELCOR analysis for these experiments provide reasonable predictions.

VI. CONCLUSIONS

Containment condensation experiments at MASLWR model facility at OSU were modeled and analyzed with MELCOR to assess the ability of MELCOR to model large scale experiments. The experiment models the containment of the conceptual MASLWR design which primarily uses condensation and natural circulation to achieve necessary energy removal from the containment in the case of accidents involving high energy steam escaping into the containment. The following conclusions are drawn from our analysis.

(1) The condensation model based on the Heat Momentum Transfer Analogy (HMTA) and diffusion theory was derived and it was demonstrated that MELCOR's condensation model agrees with the general formulations of the HMTA. This approach has been shown to provide reasonable predictions without the computational burden of first-principle based approaches.

(2) Underestimated heat flux measurements in the experiments were found to be due to the limitation posed by the locations of the thermocouples and were corrected. The ratio of the actual/expected heat flux and measured heat flux was obtained from integral energy balance and CFD simulation and the results of two different methods agree reasonable well with one another. The actual rate of heat transfer is approximately 55 ~ 75 % greater than the measured values depending on the axial locations and the prediction method. More data are needed to determine if the effect of two-dimensional heat flow is dependent on the magnitude of applied heat flux.

(3) The results show that for these two tests with substantially different noncondensable gas content provide similar heat removal rates. This is likely due to relatively low noncondensable gas fractions for both experiments, but further analysis is required confirm the noncondensable gas dependence.

(4) The analysis indicates that MELCOR is suitable in modeling the MASLWR containment condensation experiments and likely other large scale experiments based on the satisfactory predictions of the temperature-pressure response of the containment and the heat removal rate from the containment.

NOMENCLATURE

A	Area [m^2]
c	Molar density [mol/m^3]
c_p	Heat capacity [J/kg-K]
D	Mass diffusivity [m^2/s]
f	Friction factor [-]
G	Mass flux [kg/m^2-s]
H	Height [m]
h	Heat transfer coefficient [W/m^2-K]
h_m	Mass transfer coefficient [m/s]
I	Specific enthalpy [J/kg]
J	Molar flux [mol/m^2-s]
j	Transfer factor [-]
K	Mass transfer rate = $h_m\rho$ [kg/m^2-s]
k	Thermal conductivity [W/m-K]
L	Appropriate characteristic length scale [m]
M	Molar mass [g/mol]
$\dot{m}$	Mass flow rate [kg/s]
N	Number of moles [mol]
n	Normal direction vector [m]
OD	Outer diameter [cm]
P	Pressure [MPa]
q''	Heat flux [W/m^2]
R	Ratio of actual and centerline heat flux [-]
r	Position vector [m]
T	Temperature [K]
u	Velocity [m/s]
X	Mole fraction [-]
Y	Weight fraction [-]

Greek letters

α	Thermal diffusivity [m^2/s]
Δ	Difference in appropriate quantity

δ	Thickness [m]
ρ	Density [kg/m^3]
μ	Dynamic viscosity [kg/m-s]
ν	Momentum diffusivity [m^2/s]

Subscripts

a	Actual
b	Bulk
c	Condensation
d	Diffusion layer
f	Condensate film
fg	Vaporization
g	Noncondensable gas
H	Heat transfer
i	Liquid-vapor interface
j	Appropriate state
M	Mass transfer
m	Measured value
o	Initial state
p	Heat transfer plate
s	Steam
ss	Quasi steady state

Dimensionless Numbers

Nu	Nusselt number = hL/k
Pr	Prandtl number = $\nu/\alpha = c_p\mu/k$
Re	Reynolds number = $\rho uL/\mu$
Sc	Schmidt number = $\nu/D = \mu/\rho D$
Sh	Sherwood number = h_mL/D

LIST OF TABLES AND FIGURES

Table 1. Dimensions of containment structure components [1]

Table 2. Initial and steady state conditions of containment condensation tests

Table 3. Reported uncertainties for heat flux measurements

Table 4. Comparison of heat and mass transfer parameters

Table 5. Average heat flux at different axial locations. Heat flux in kW/m^2

Table 6. Integral heat balance with incoming steam. Heat flux in kW/m^2

Figure 1. Containment structure of OSU MASLWR facility

Figure 2. Top view of the containment structures; outer vessel diameter marked

Figure 3. Side view of the containment structures and the control volume representation; dimensions in meters

Figure 4. Containment pressure and inlet steam flow rate for Test 1

Figure 5. Containment pressure and temperature for Test 1

Figure 6. Containment pressure and temperature for Test 2

Figure 7. Heat flux at elevation 4.82 m for Test 1

Figure 8. Heat flux ratio for both test at different axial locations; averaged value is 1.63

Figure 9. Cross-sectional view of the CPV system in scale; thermocouples marked as black dots

Figure 10. Ratio calculated from integral energy balance; hollow pts, ratio; solid pts, % difference

Figure 11. Temperature contour map of the CPV during quasi steady state for Test 1

Figure 12. Heat flux ratio calculated by CFD

Figure 13. Corrected heat flux at different axial locations, Test 1; ●, Original data

Figure 14. Corrected heat flux at different axial locations, Test 2; ●, Original data

Table 1. Dimensions of containment structure components [1]

Structure		*OD* [cm]	*H* [m]
HPC	Lower cylindrical section	27.0	3.87
	Eccentric cone section	27.0 – 50.8	0.508
	Upper cylindrical section	50.8	1.21
CPV		76.2	7.37

Table 2. Initial and steady state conditions of containment condensation tests

	Input steam		Initial condition		Steady state condition			
	P [MPa]	T [K]	P [MPa]	T [K]	P [MPa]	T [K]	X_g [-]	Y_g [-]
Test 1	2.0684	526.48	0.0076	288.26	1.486	483.76	0.008	0.013
Test 2			0.1029	298.15	1.580	484.10	0.104	0.157

Table 3. Reported uncertainties for heat flux measurements

	σ	Unit
k	0.6 [24]	W/m-K
T	1.1 [1]	K
δ	0.05	mm

Table 4. Comparison of heat and mass transfer parameters

Parameter	Heat transfer	Mass transfer
Transfer coefficient	h [W\m^2-k]	h_m [m/s]
Diffusivity	α [m^2-s]	D [m^2/s]
Transferred quantity	h/c_p [kg/m^2-s]	K [kg/m^2-s]
Ratio to momentum transfer	Pr	Sc
Ratio of convective and diffusive transfer	Nu	Sh

Table 5. Average heat flux at different axial locations. Heat flux in kW/m^2

Measurement location		Test 1			Test 2		
	Elevation [m]	MELCOR	Experiment	Ratio [-]	MELCOR	Experiment	Ratio [-]
1	2.22	46.012	27.843	1.65	43.034	27.329	1.57
2	2.92	45.613	26.954	1.69	44.664	26.608	1.68
3	3.82	45.633	28.234	1.62	44.687	27.071	1.65
4	4.82	44.960	28.106	1.60	44.177	26.677	1.66
5	5.31	45.509	29.799	1.53	44.720	27.270	1.64
Mean				1.62			1.64
		1.63					

Table 6. Integral heat balance with incoming steam. Heat flux in kW/m^2

Measurement location		Test 1			Test 2		
	Elevation [m]	Energy balance	Experiment	Ratio [-]	Energy balance	Experiment	Ratio [-]
1	2.22	48.827	27.843	1.75	41.854	27.329	1.53
2	2.92	48.828	26.954	1.81	41.578	26.608	1.56
3	3.82	48.878	28.234	1.73	41.560	27.071	1.54
4	4.82	48.239	28.106	1.72	40.023	26.677	1.50
5	5.31	48.259	29.799	1.62	41.164	27.270	1.51
Mean				1.73			1.53
		1.63					

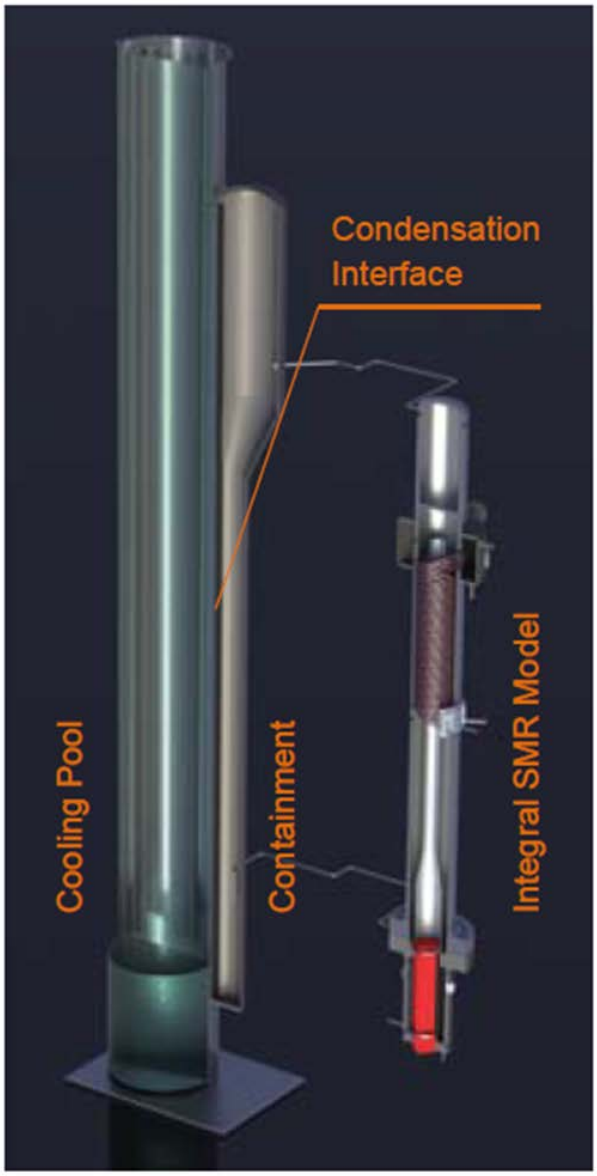

Fig. 1. Containment structure of OSU MASLWR facility

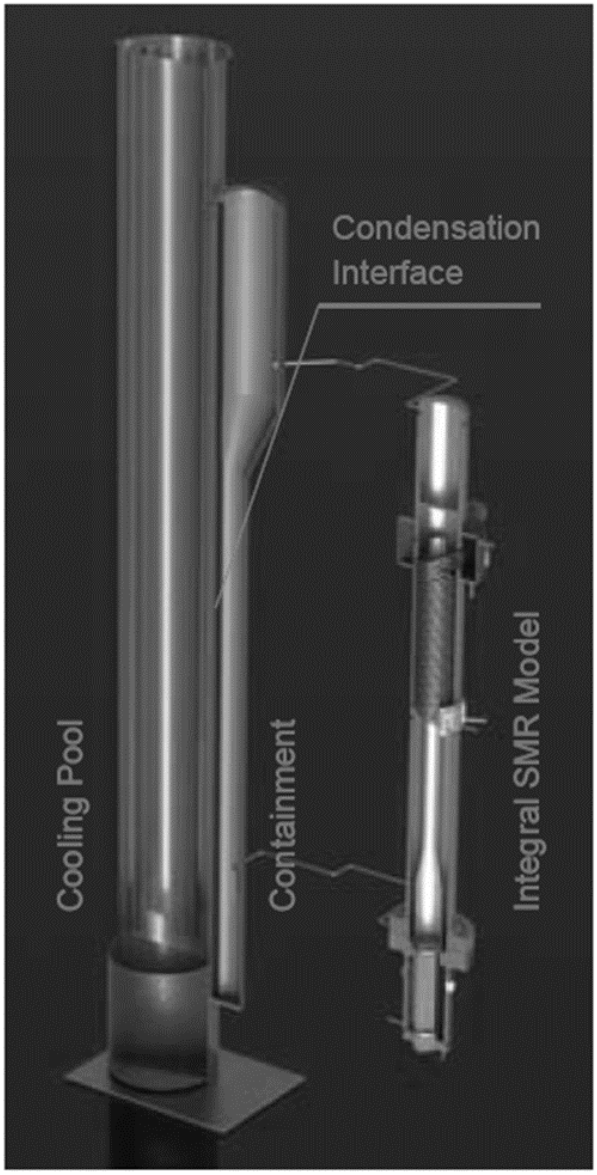

<Figure 1 in grayscale for print>

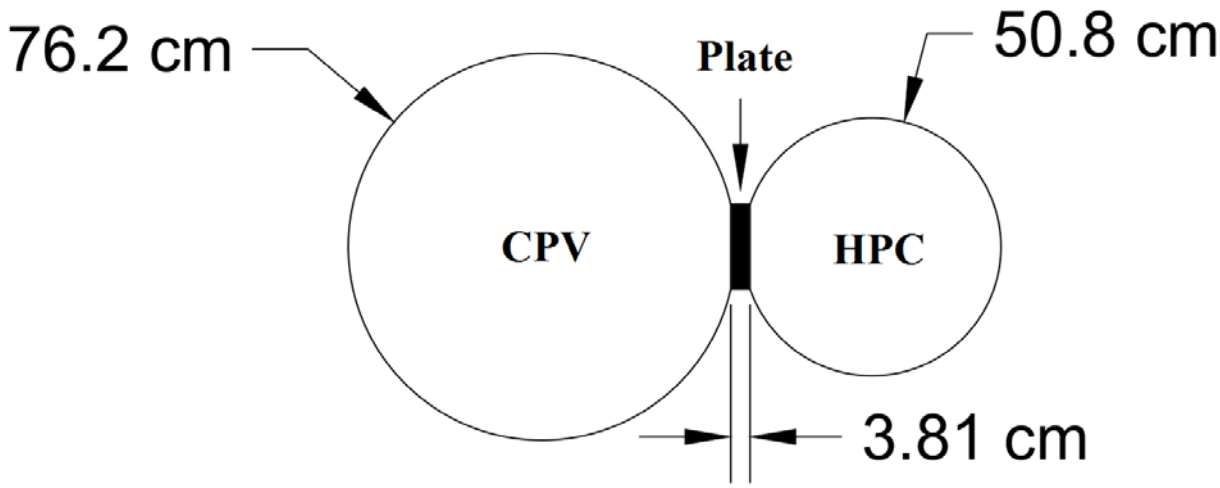

Fig. 2. Top view of the containment structures; outer vessel dimeter marked

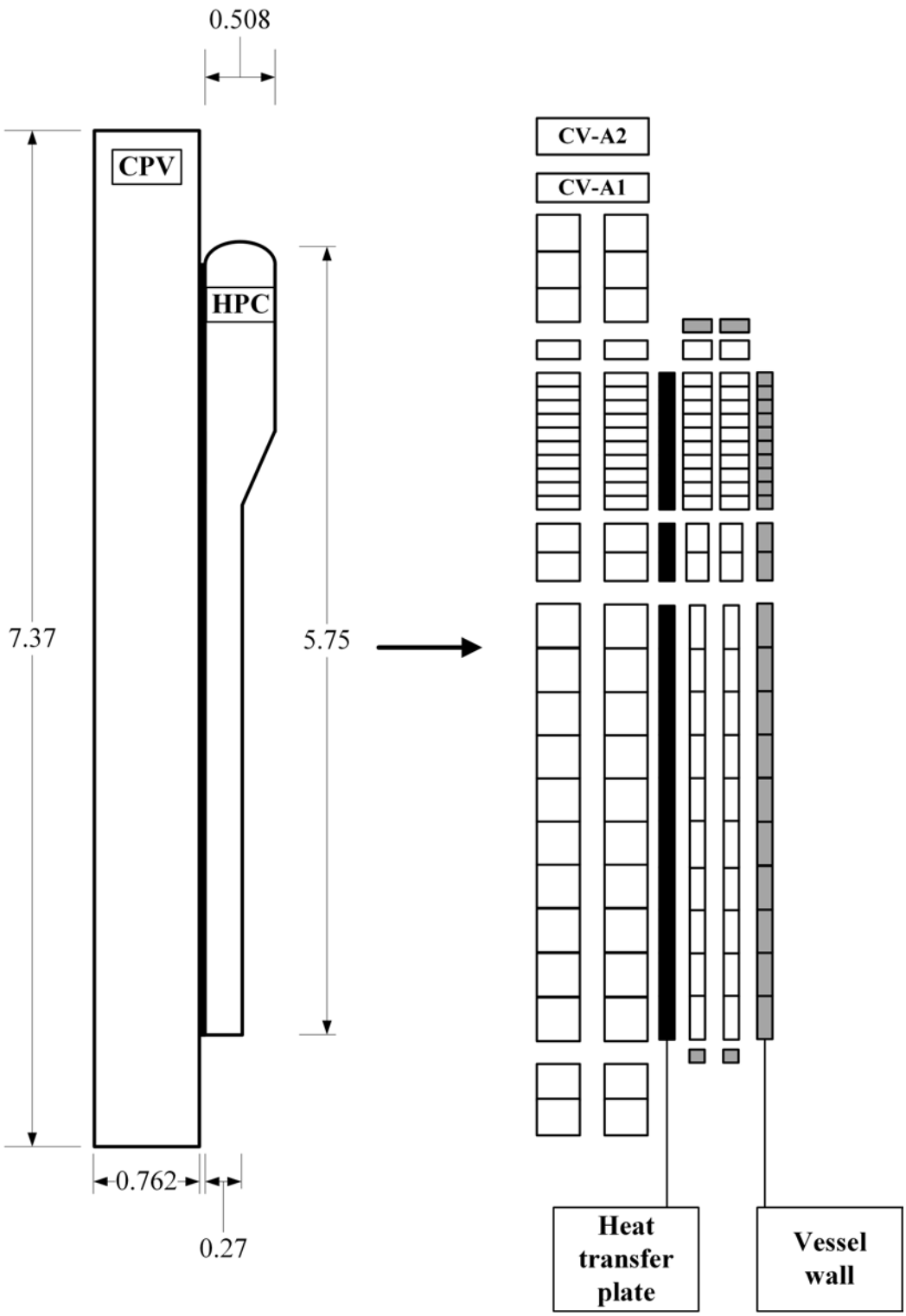

Fig. 3. Side view of the containment structures and the control volume representation; dimensions in meters

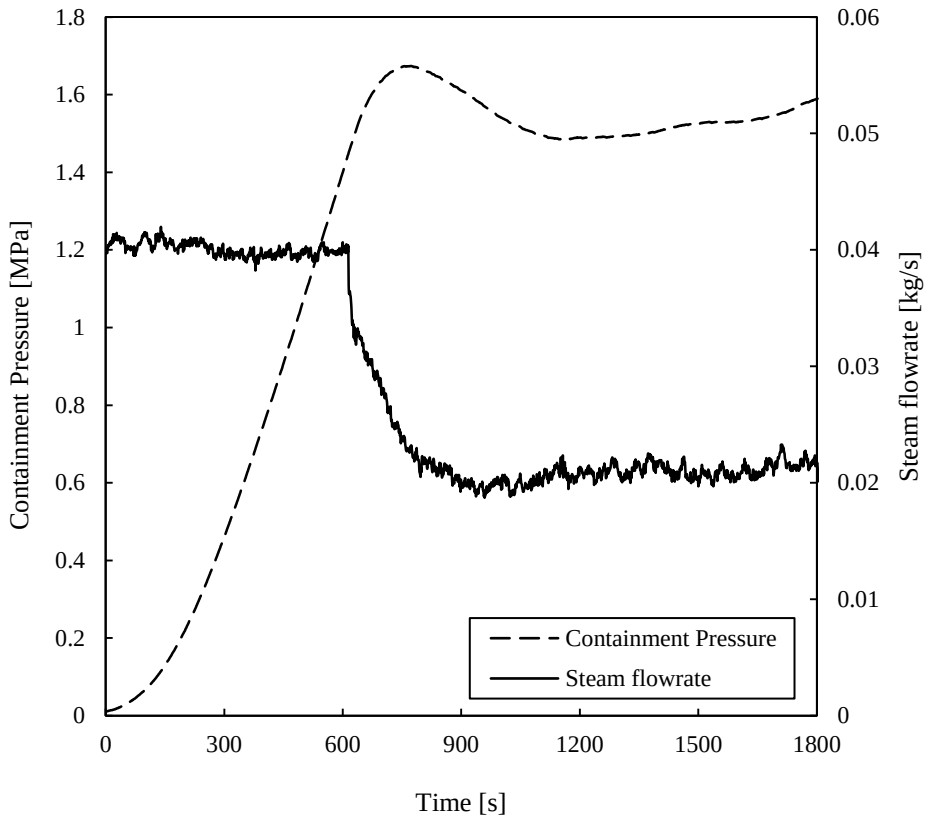

Fig. 4. Containment pressure and inlet steam flow rate for Test 1

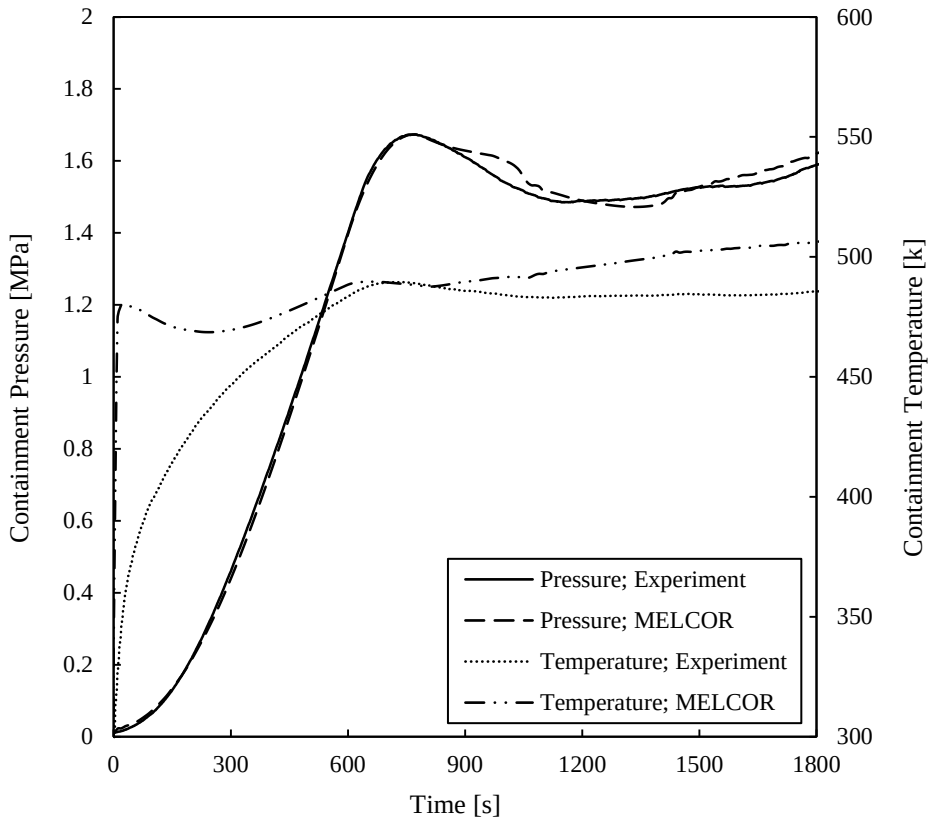

Fig. 5. Containment pressure and temperature for Test 1

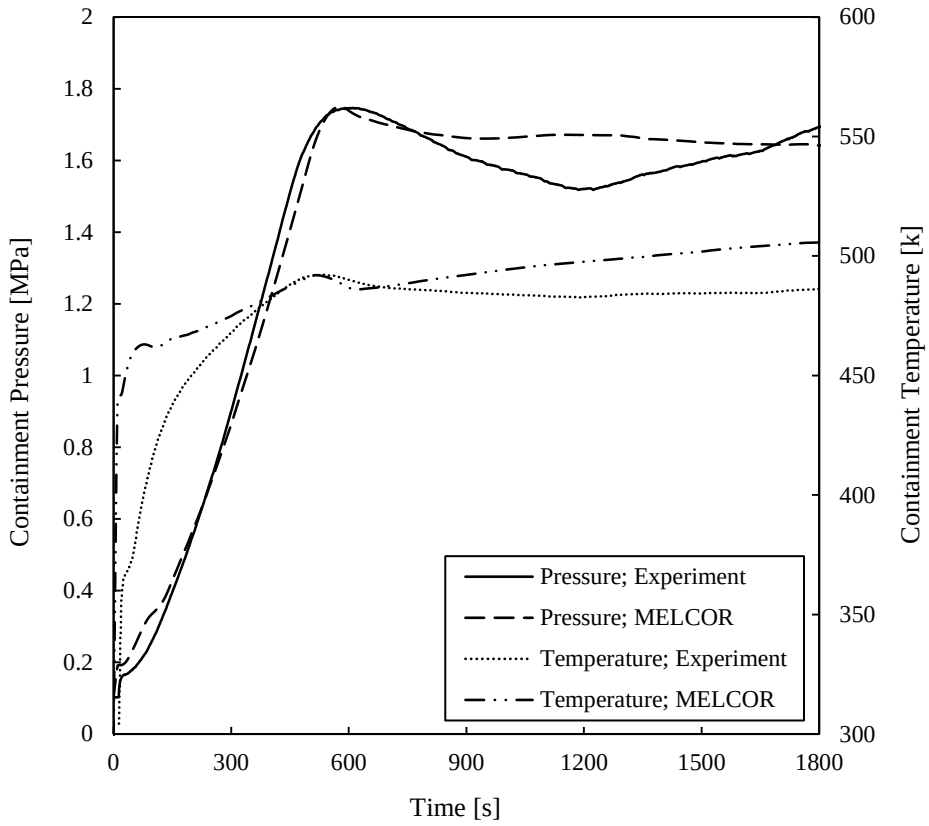

Fig. 6. Containment pressure and temperature for Test 2

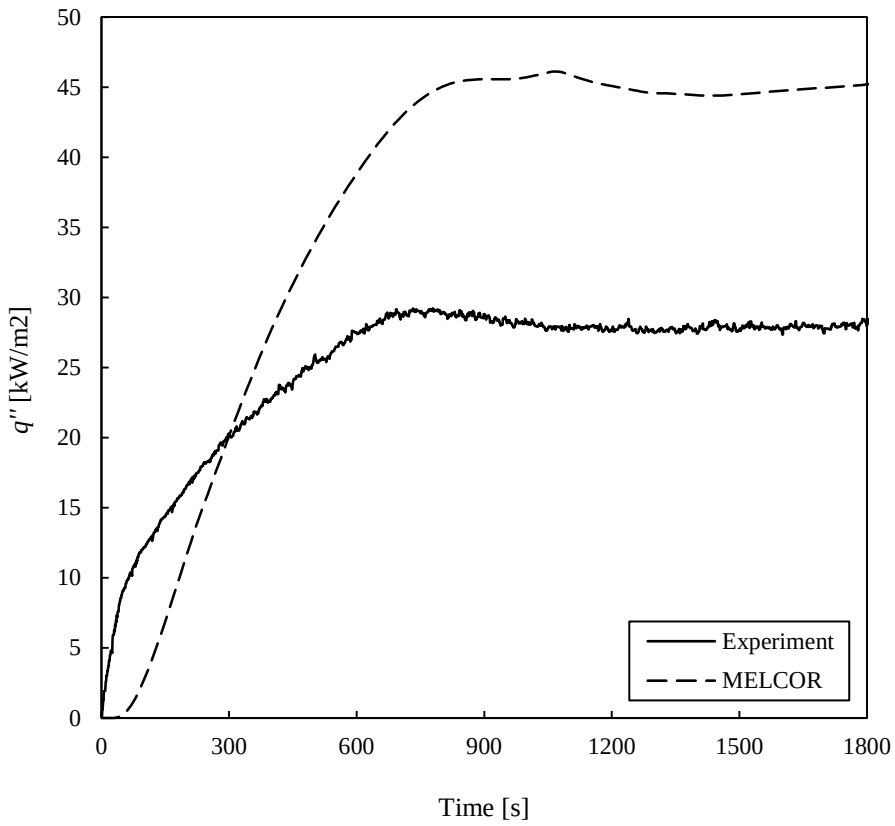

Fig. 7. Heat flux at elevation 4.82 m for Test 1

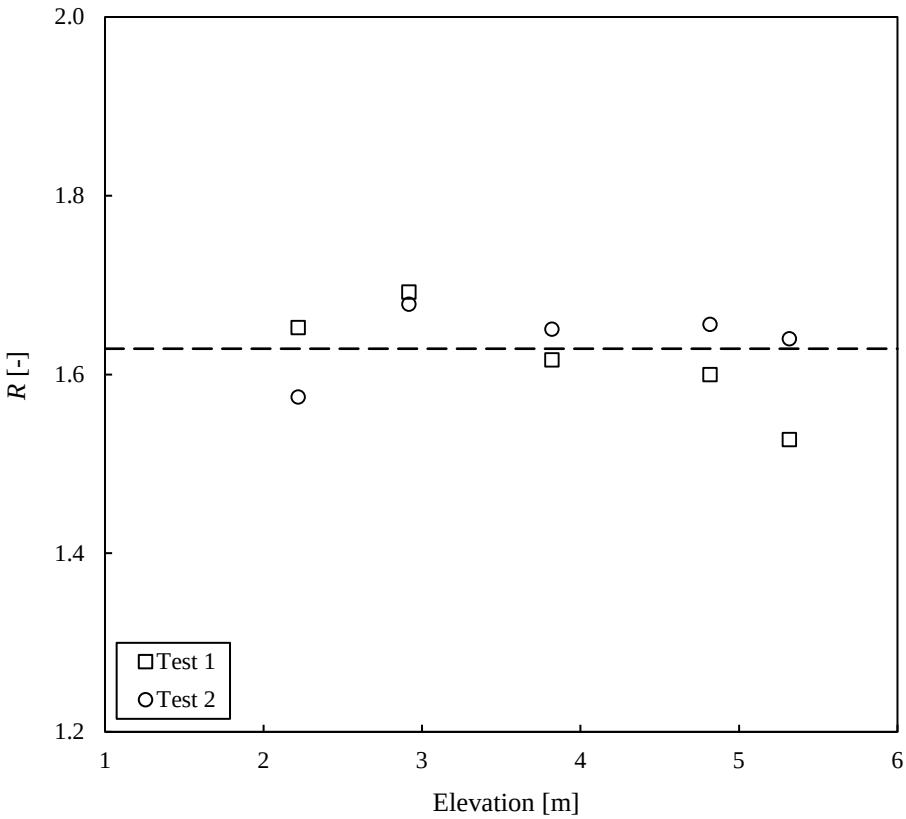

Fig. 8. Heat flux ratio for both test at different axial locations; averaged value is 1.63

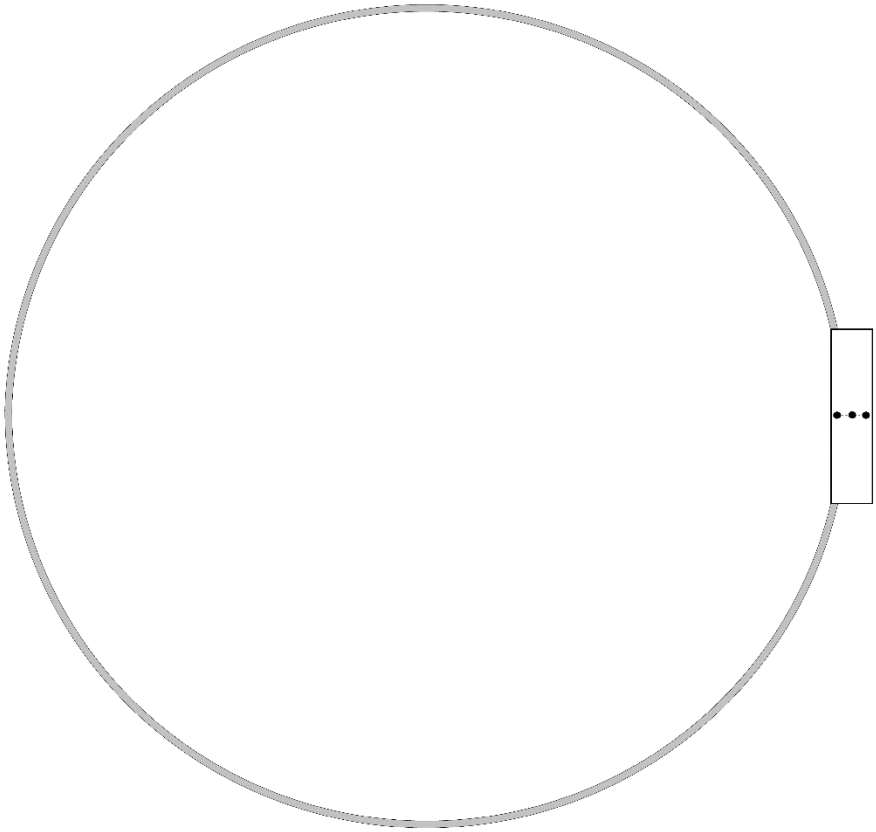

Fig. 9. Cross-sectional view of the CPV system in scale; thermocouples marked as black dots

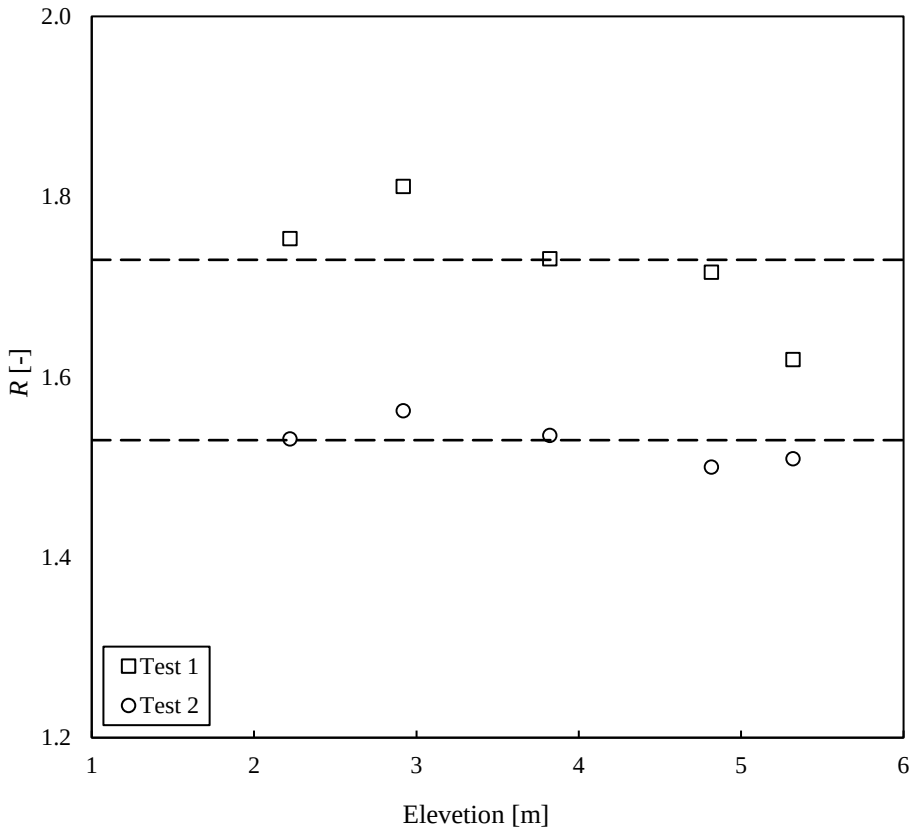

Fig. 10. Ratio calculated from integral energy balance

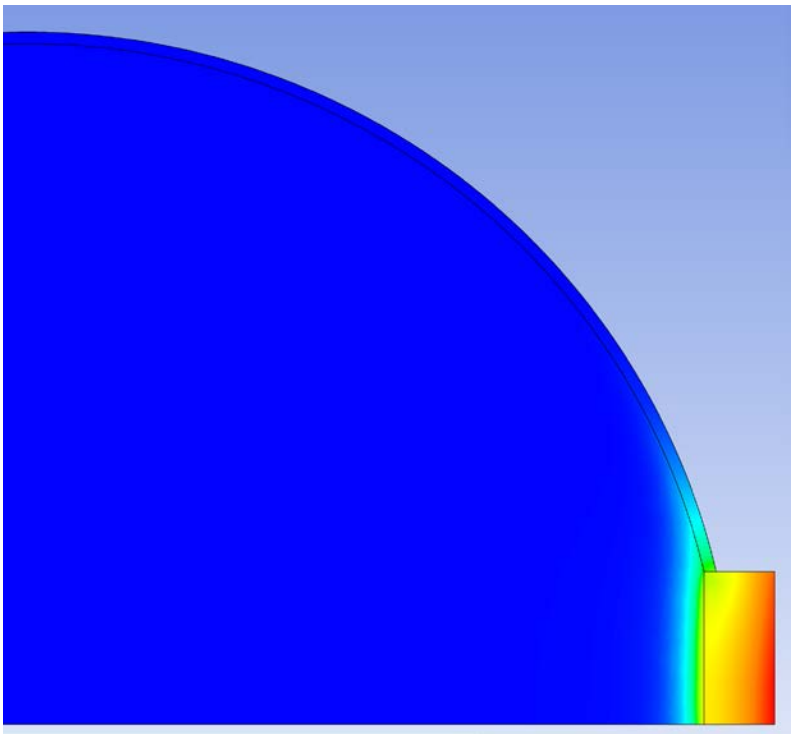

Fig. 11. Temperature contour map of the CPV during quasi steady state for Test 1

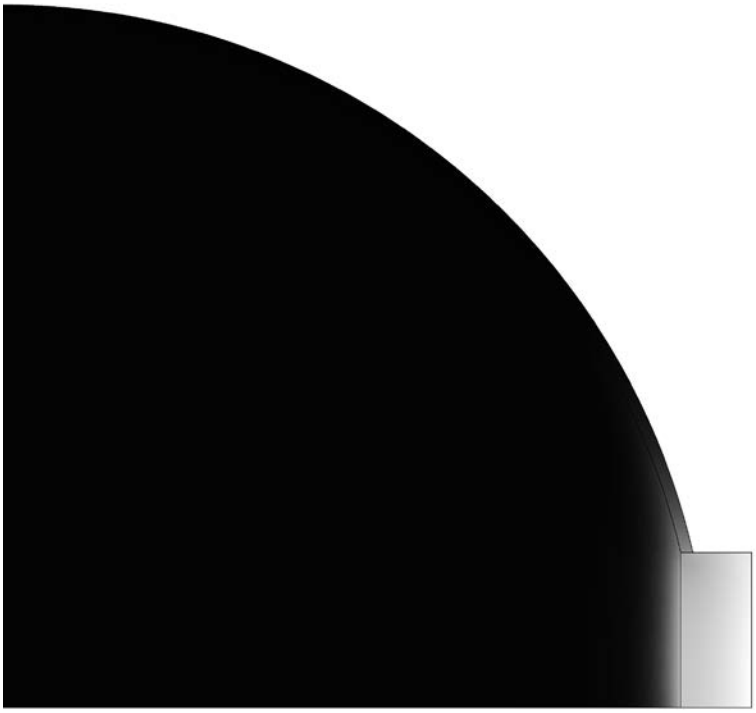

<Figure 11 in grayscale for print>

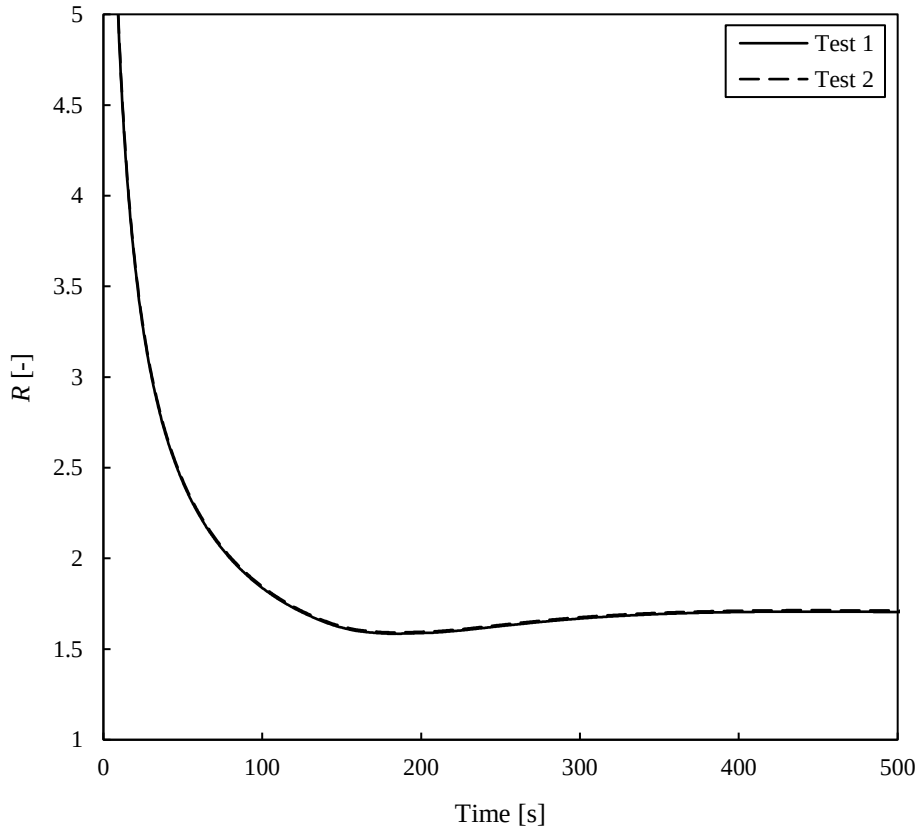

Fig. 12. Heat flux ratio calculated by CFD

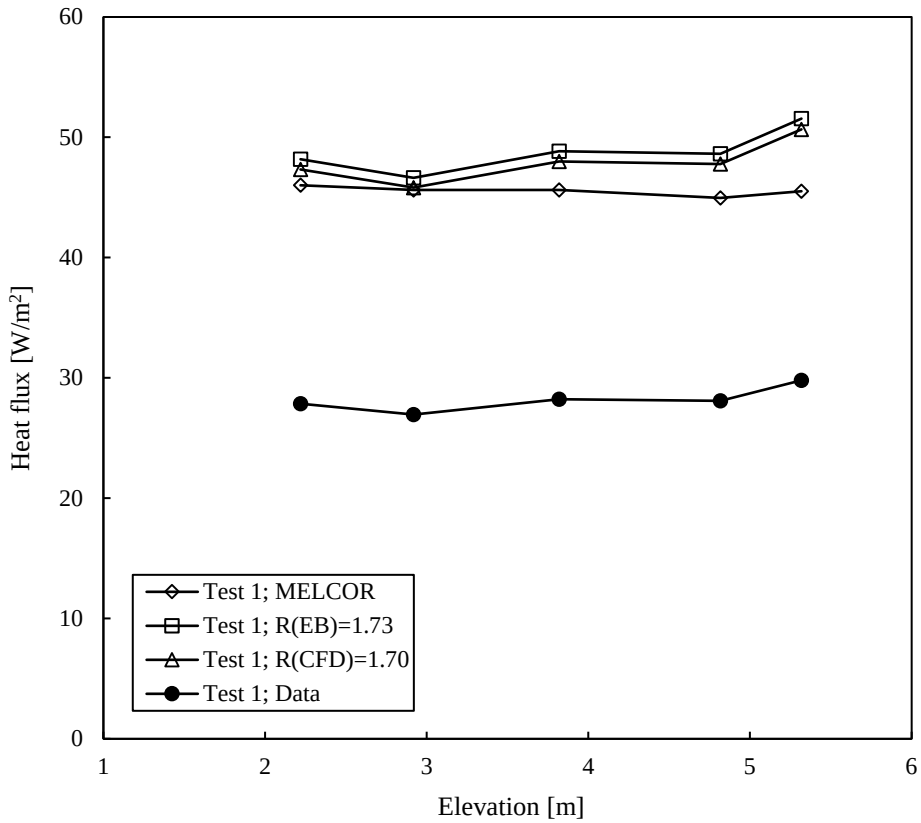

Fig. 13. Corrected heat flux at different axial locations, Test 1; ●, Original data

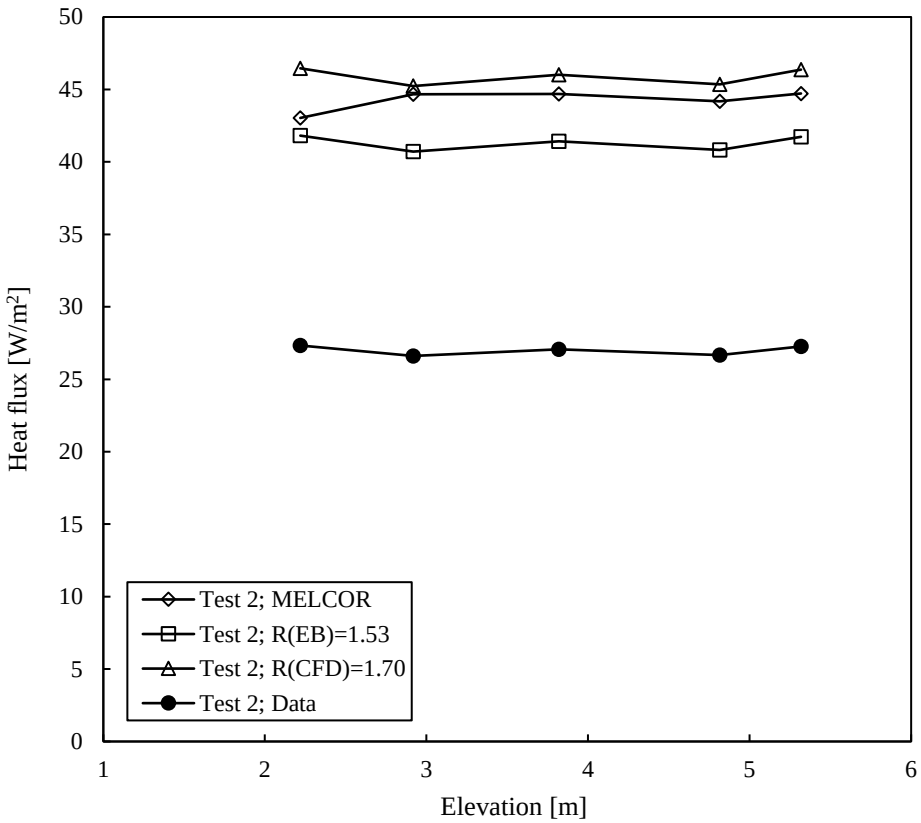

Fig. 14. Corrected heat flux at different axial locations, Test 2; ●, Original data

REFERENCES

1. M. R. Galvin, C. J. Bowser, "OSU MASLWR Test Facility Modification Description Report," IAEA Contract Number USA-13386, Oregon State University (2010).

2. D. F. Othmer, "The Condensation of Steam," *Ind. Engr. Chem.*, **21**, 576 (1929).

3. W. A. Nusselt, "The Surface Condensation of Water Vapor," *Zetrschr. Ver. Ing.*, **60**, 541-546. (1916)

4. E. M. Sparrow, S. H. Lin, "Condensation Heat Transfer in the Presence of a Noncondensable Gas," *J. Heat Transfer*, **86**, 430 (1964).

5. C. G. Kirkbride, "Heat Transfer by Condensing Vapor on Vertical Tubes," *Trans. AIChE*, **30**, 170. (1933).

6. R. A. Seban, "Remarks on Film Condensation with Turbulent Flow," *Trans. ASME*, **76**, 299. (1954).

7. W. M. Rohsenow, "Heat Transfer and Temperature Distribution in Laminar Film Condensation," *Trans. ASME*, **78**, 1645-1648. (1956).

8. A. E. Dukler, "Fluid Mechanics and Heat Transfer in Vertical Falling Film Systems," *Chem. Eng. Progr., Symposium Ser.*, **30**, 1-10. (1960).

9. J. Lee, "Turbulent Film Condensation," *AIChE J.*, **10**. 540-544. (1964).

10. P. F. Peterson, V. E. Schrock, T. Kageyama, "Diffusion Layer Theory for Turbulent Vapor Condensation with Noncondensable Gases," *J. Heat Transfer*, **115**, 998 (1993).

11. L. E. Herranz, M. H. Anderson, M. L. Corradini, "A Diffusion Layer Model for Steam Condensation within the AP600 Containment," *Nucl. Engr. Des.*, **183**, 133 (1998).

12. Y. Liao, K. Vierow, "A Generalized Diffusion Layer Model for Condensation of Vapor with Noncondensable Gases," *J. Heat Transfer*, **129**, 988 (2007).

13. T. H. Chilton, A. P. Colburn, "Mass Transfer (Absorption) Coefficients: Prediction from Data on Heat Transfer and Fluid Friction," *Ind. Engr. Chem.*, **26**, 1183 (1934).

14. R. B. Bird et al., *Transport Phenomena*, Wiley and Sons Inc., New York (1960).

15. D. Butterworth et al., *Two-Phase Flow and Heat Transfer*, Oxford University Press (1977).

16. J. G. Collier et al., *Convective Boiling and Condensation*, McGraw Hill, London (1972).

17. M. L. Corradini, "Turbulent Condensation on a Cold Wall in the Presence of a Noncondensable Gas," *Nucl. Tech.*, **64**, 186-195. (1984).

18. S. S. Kutateladze, I. I. Gogonin, "Heat Transfer in Film Condensation of Slowly Moving Vapour," *Int. J. Heat Mass Transfer*, **22**, 193 (1979).

19. J. C. de la Rosa, L. E. Herranz, J. L. Munoz-Cobo, "Analysis of the Suction Effect on the Mass Transfer When Using the Heat and Mass Transfer Analogy," *Nucl. Engr. Des.*, **239**, 2042 (2009).

20. W. Ambrosini, N. Forgione, A. Manfredini, F. Oriolo, “On Various forms of the Heat and Mass Transfer Analogy: Discussion and Application to Condensation Experiments,” *Nucl. Engr. Des.*, **236**, 1013 (2006).

21. W. Fu, D. S. Yoon, M. L. Corradini, “Assessment of the MELCOR and RELAP5-3D Code for Condensation in the Presence of Noncondensable Gas,” *International Topical Meeting on Nuclear Reactor Thermal Hydraulics 2015, Chicago, USA*. Aug 30 – Sept 4, 2015.

22. S. M. Modro et al., “Multi-Application Small Light Water Reactor Final Report,” DOE Nuclear Energy Research Initiative Final Report, Idaho National Engineering and Environmental Laboratory (2003).

23. J. N. Reyes, J. King, “Scaling Analysis for the OSU Integral Test Facility,” Oregon State University (2003).

24. B. F. Blackwell et al., “Uncertainty Estimation in the Determination of Thermal Conductivity of 304 Stainless Steel,” *Proceedings of IMECE '*, 2000

25. R. O. Gauntt et al., “MELCOR computer code manuals,” NUREG report, U.S. NRC, NUREG/CR-6119 (2005).